SDC-91-00081

SDC
SOLENOIDAL DETECTOR NOTES

$Z^{\circ} \rightarrow$ Hadrons in SDC

A. B. Wicklund

30 AUGUST 1991

ANL-HEP-TR-91-74

SDC-91-00081
August 30, 1991

$Z^0 \rightarrow$ Hadrons in SDC

A. B. Wicklund

We report on a study of hadronic Z^0 decays at high P_t (P_t >500 GeV/c), at 40 TeV CM energy. [1] Our goal here is to understand the effects of the kinematics of Z^0 decay, especially the Lorentz boost, on detection issues. We used an ISAJET sample of Drell Yan events, requiring the Z^0 to have pseudorapidity (η) in [-1.5,1.5] and P_t>500 GeV/c. ISAJET forces the Z^0 to decay to two primary partons, which then cascade by gluon and quark emission to stable hadrons. We excluded $Z^0 \rightarrow \nu\bar{\nu}$ decays. In about 10 % of the hadronic decays, significant energy is lost due to neutrino emission from heavy quarks, so that the hadronic mass is significantly less than the Z^0 mass generated; these events were not explicitly removed. We treated muons like other hadrons, assuming that high P_t muons could be identified and corrected for. For this study we retained only the stable daughter particles in Z^0 decay, labelled according to their parton parentage (" Jet 1 or 2"). We ignored the particles from the underlying event and from other final state jets. (These contributions, along with other non-Z^0 "noise", can be explicitly added back for relevant studies.) Finally, we note that the Z^0 decay angular distribution is approximately flat for these events, not peaked at 90 deg. as in Higgs$\rightarrow Z^0Z^0$; this will have little effect on our conclusions. To avoid very asymmetric decays, we required each of the two jets to satisfy P_t> 100 GeV/c.

The most striking feature of these events is the strong pencil-like collimation of the jets, due to the Lorentz boost. Figure 1 shows the E_t flow relative to the jet axes in η-ϕ space; (a,c) are for the slower jet, (b,d) the faster. We have defined axes in η-ϕ space such that "parallel" denotes a direction pointing from the slow jet to the fast jet in η-ϕ space; "perpendicular" is the orthogonal direction. The E_t flow is highly collimated in both projections, and most of the E_t is confined to $\pm.04$ ($\pm.08$) units for the fast (slow) jets. Of course, this collimation may be smeared out by calorimeter transverse leakage and magnetic field sweeping. Figure 2 shows the P_t spectrum for hadrons and photons, weighted by E_t. Most of the energy is carried by photons or by hadrons above 6 GeV/c, so we would expect rather little smearing from the magnetic field for these events. Figure 3 shows the E_t flow along the same axes, for all hadrons. Figure 3 differs from fig. 1 in that the distance is measured from the overall Z^0 axis, rather than from the individual jet axes. The collimation along the "perpendicular" axis is unchanged, but the two jets are separated by 0.3 units along the "parallel" axis (fig. 3a). The separation of the jets along the "parallel" axis is smeared by the Z^0 decay distribution,

[1] This report was originally prepared in Sept. 1990; for recent related analyses see R. Blair et al., SDC-90-00150, and A. Para et al., SDC-90-00149.

so the hadronic E_t flow is broadened. The shaded portion of fig.3a shows the E_t flow of the partons from the "fast jet" alone; it is clear that the remnants of the fast and slow jets are well separated by $\eta_{||} = 0$. Thus, depending on the Z^0 decay angle, each event appears as two pencil jets, each around 0.03 in radius, separated by 0.3 in η-ϕ space.

The strong jet collimation and two-lobed structure should be useful in separating signal from background, and suggests the importance of fine granularity in both the EM and HAD calorimeters. Each lobe should be linked to a tight cluster of high P_t tracks, and a finely collimated photon shower profile (This could be measured quite accurately in a shower-max detector in the EM). Clearly a denser calorimeter would help to minimize lateral hadronic shower leakage.

In addition to signal identificaton, the jet collimation suggests that the Z^0 mass determination should be quite sensitive to the jet angular resolution, which might be improved using information from the tracking chambers (charged track energy flow) and from the photon detector at shower max. For example, we can define the Z^0 mass by

$$M^2 = 2E_1E_2[1 - cos(\theta)] \sim E_1E_2\theta^2$$

where θ is the separation in η, ϕ space, and E_1, E_2 are the measured energies of the two lobes. In that case, it is straightforward to calculate the resolutions on E and θ that would correspond to the natural width of the Z^0, eg σ (M)= $\Gamma/2$ (σ(M)/M= 0.014). These are

$$d(E)/E = 0.019$$

$$d(\eta_{||}) = 0.003$$

at 250 GeV. In practice, this simple calculation is misleading, because it ignores the intrinsic masses of the two jets. In the ISAJET fragmentation, the average jet mass is 16 GeV, with a broad (σ(Mjet)$\sim$ 6 GeV) distribution. To lowest order in M/E, this leads to

$$M^2 \sim E_1E_2\theta^2 + M_1^2(1 + E_2/E_1) + M_2^2(1 + E_1/E_2)$$

The additional mass terms affect the Z^0 mass and resolution.

We tried computing M(Z^0) in several ways. We first divided the calorimeter into fixed cells, and summed the cells in the usual fashion to define a four-vector for the total dijet cluster. We assumed that the particle energy was recorded perfectly in the calorimeter, and each calorimeter cell (summed over particle energies) was used to define a vector (direction defined by η, ϕ at cell center). Thus, each cell defines a (massless) 4-vector contribution to the Z^0. The cell sum was used to define the Z^0 mass. In addition, we tried the simple (massless) jet definition, using the exact energy of each jet, and the exact opening angle between the jets. These calculations are compared in fig. 4a (cell algorithm, using cell size 0.05X0.05), and 4b (simple massless jet result). The cell algorithm gives much better resolution than the massless result:

$$M = 88.6, \sigma = 2.6(cell = .05)$$

$$M = 79.0, \sigma = 8.0(masslessjets)$$

where σ is the rms of the difference between calculated and generated Z^0 masses. We emphasize that the "massless jet" algorithm would give perfect resolution if we added back the true jet masses in the calculation- it illustrates the effect of the jet masses alone on M_Z and σ (M_Z). The cell algorithm implicitly includes the jet masses, but suffers from the finite cell segmentation. It may seem surprising that the cell algorithm works so well; one might expect that it would give poor resolution on the intrinsic jet masses, since most of the jet E_t is confined to one cell, and that it would give poor opening angle (θ) resolution due to the segmentation. The fact that it gives adequate jet mass resolution is explained below. We remark that, with perfect calorimeter energy response, the 0.05X0.05 cell algorithm gives ± 0.007 resolution on θ (only twice the 0.003 criterion set by the natural Z^0 width.) We tried using the photon contribution to each jet, assuming a perfect shower max detector, and compared the opening angle between the photon components with the full jets. The resolution on θ using the photons alone is ± 0.027, much worse than the 0.05 cell result. Evidently, the fluctuations between photon and hadron components are large enough that a perfect shower max photon detector would give worse resolution on the jet direction than a relatively coarse EM+HAD calorimeter. Of course, lateral hadronic shower spreading may affect this result, but it is not clear whether it would make the θ resolution better or worse.

Turning to the question of jet mass resolution, note that the intrinsic jet mass can be approximated (after some algebra) by forming a sum over stable hadrons of

$$M^2 \sim \sum_i E_i \times \sum_i [E_i(d\eta^2 + d\phi^2)]$$

where dη and dϕ are the distances between the hadron and the jet axis. This expression ignores the hadron mass. Figure 5 shows the distribution of the quantity $E_t(d\eta^2 + d\phi^2)$ for all hadrons, as a function of the distance from the jet axis, measured along the "parallel" direction. Figure 5 (a) and (b) are for the slow and fast jets respectively. In each case the area of the distribution corresponds to the jet mass. Thus, even though most of the E_t flow in each jet is confined to $\pm .04$ units in eta (see fig. 1), it is necessary to integrate well beyond this limit, out to ± 0.3 at least, to get the full jet mass. This explains why the cell algorithm gives good jet mass, and hence good M(Z^0) resolution. Even though 0.05 is a coarse cell size for observing the E_t flow, it is a good match to the mass determination. From the width of these "mass flow" plots, one would guess that lateral shower spreading in the calorimeter ($\pm .05$) would not affect the jet mass resolution to first order.

Figure 6 shows a similar plot for the Z^0 mass. It shows the distribution of $E_t(d\eta^2 + d\phi^2)$ for hadrons as a function of the distance "R" from the Z^0 axis. The integral of the plot is proportional to the Z^0 mass. Thus, if one simply summed over cells out to a fixed radius from the Z^0 axis (ie, the weighted mean of the two jet axes), then one would need to go out to R$\sim$0.6 to get most of the Z^0 mass. This reflects the jet results above- the jets are separated by 0.3 units, and one must cover a region of radius R$\sim$0.3 around each jet, to get good jet masses.

The cell size is an important parameter in the Z^0 resolution, because it affects both the opening angle, θ, and the jet masses. With perfect calorimeter response, the variation of Z^0 mass resolution with cell size is as follows:

Cell Size	Z Mass Resolution
0.20	13.3 GeV
0.10	4.6 GeV
0.05	2.6 GeV
0.025	1.6 GeV

The resolution eventually bottoms out on the fact that we ignore the masses of the hadrons (each cell is treated as a massless parton with E=p= sum over hadron energies). Evidently 0.05 is already coarser than the Z^0 natural width (± 1.25 GeV).

We can also impose a cutoff on η, ϕ for the cells used in the Z^0 reconstruction. If we retain hadrons that are within a fixed cut from either jet axis ($\pm\eta_{cut}$ in each direction), we get

Cut	M(Z^0)	σ(M)
none	88.6	2.6
0.60	88.4	2.9
0.30	87.5	3.1
0.15	81.8	3.9
0.04	48.5	24.9

It is clear that the mass resolution will be sensitive to the "noise" from underlying event, pile-up, etc, since the particles at large distance from the jet axes have a big effect on the Z^0 mass. It would be desirable to minimize the above cut, but it appears to be impractical to go much below 0.3. Figure 7 compares the Z^0 mass distributions using a cut at 0.3 (a) for perfect calorimeter resolution and 0.05 cell size, and (b) adding nominal energy resolution as follows:

$$\sigma(E) = 0.15\sqrt{E} + 0.01 \quad \gamma's$$
$$\sigma(E) = 0.50\sqrt{E} + 0.03 \quad Hadrons$$
$$\sigma(E) = \pm 1.0 GeV \quad (\text{"}cellnoise\text{"})$$

Here we have added the constant terms in quadrature, for each particle. The resolution smearing affects the resolution, but the kinematical limitations alone (from the cell size, and the 0.3 cut) are relatively big effects even with perfect resolution.

To summarize, we show that *detection* of high P_t $Z^0 \rightarrow$ hadrons depends critically on having good lateral segmentation, to guarantee sensitivity to the collimated jet structure. In addition, *measurement* of the Z^0 mass is sensitive not only to the energy and angle resolution on the jets, but also to the jet masses. The kinematics are such that the Z mass resolution

and the jet masses themselves are well determined with cells of size 0.05 or smaller. However, the resolution depends on good measurement of the small energy depositions outside of the jet cores, at least out to 0.3 units of R from each jet core. With canonical assumptions on resolution and noise, we get reasonable (± 5 GeV) Z^0 mass resolution. The use of auxiliary information from central tracking and fined grained photon detection at shower max, should be useful; however, the photon information alone does not provide adequate resolution on the jet angles to improve the mass resolution. Finally, we emphasize that in defining the lateral segmentation, we have assumed an ideal calorimeter. Lateral spreading of hadron showers in the calorimeter will place a natural limit on the optimal segmentation and achievable resolution; this will be the subject of a subsequent report.

Figure Captions

1. Et flow for slow (a,c) and fast jets (b,d) measured in coordinate system as described in text.

2. Pt spectra for (a) γ's and (b) hadrons, weighted by particle Et; the integral, diveded by number of events, gives the total Et for the Z^0.

3. Et flow along (a) parallel and (b) perpendicular axes as defined in text; shaded area shows Et flow from particles in the fast jet alone.

4. Jet-jet invariant mass (a) using sum over .05X.05 calorimeter cells, and (b) using the exact energy and opening angle between each jet, ignoring the jet masses.

5. Et flow, weighted by R^2, for particles in (a) slow and (b) fast jets, projected along the parallel axis.

6. Et flow, weighted by R^2, for particles from Z^0 decay, measured with respect to the Z^0 axis; the integrated area is proportional to the Z^0 mass.

7. Jet-jet mass distribution for .05X.05 cell algorithm (a) with no resolution smearing, and (b) with smearing as prescribed in text.

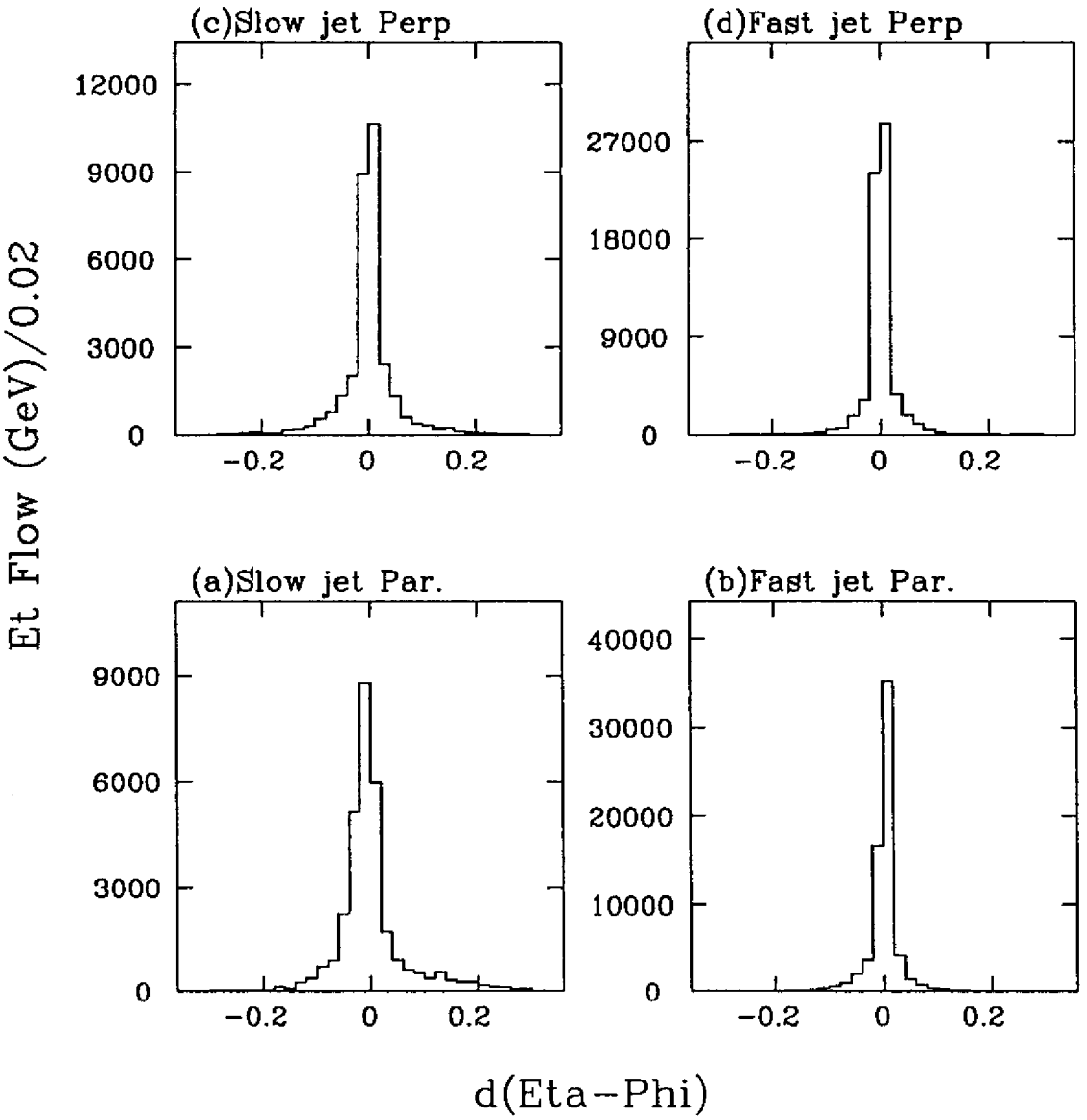
(c)Slow jet Perp
(d)Fast jet Perp
(a)Slow jet Par.
(b)Fast jet Par.
Et Flow (GeV)/0.02
d(Eta−Phi)
12000
9000
6000
3000
0
27000
18000
9000
40000
30000
20000
10000
−0.2
0
0.2

Figure (1)

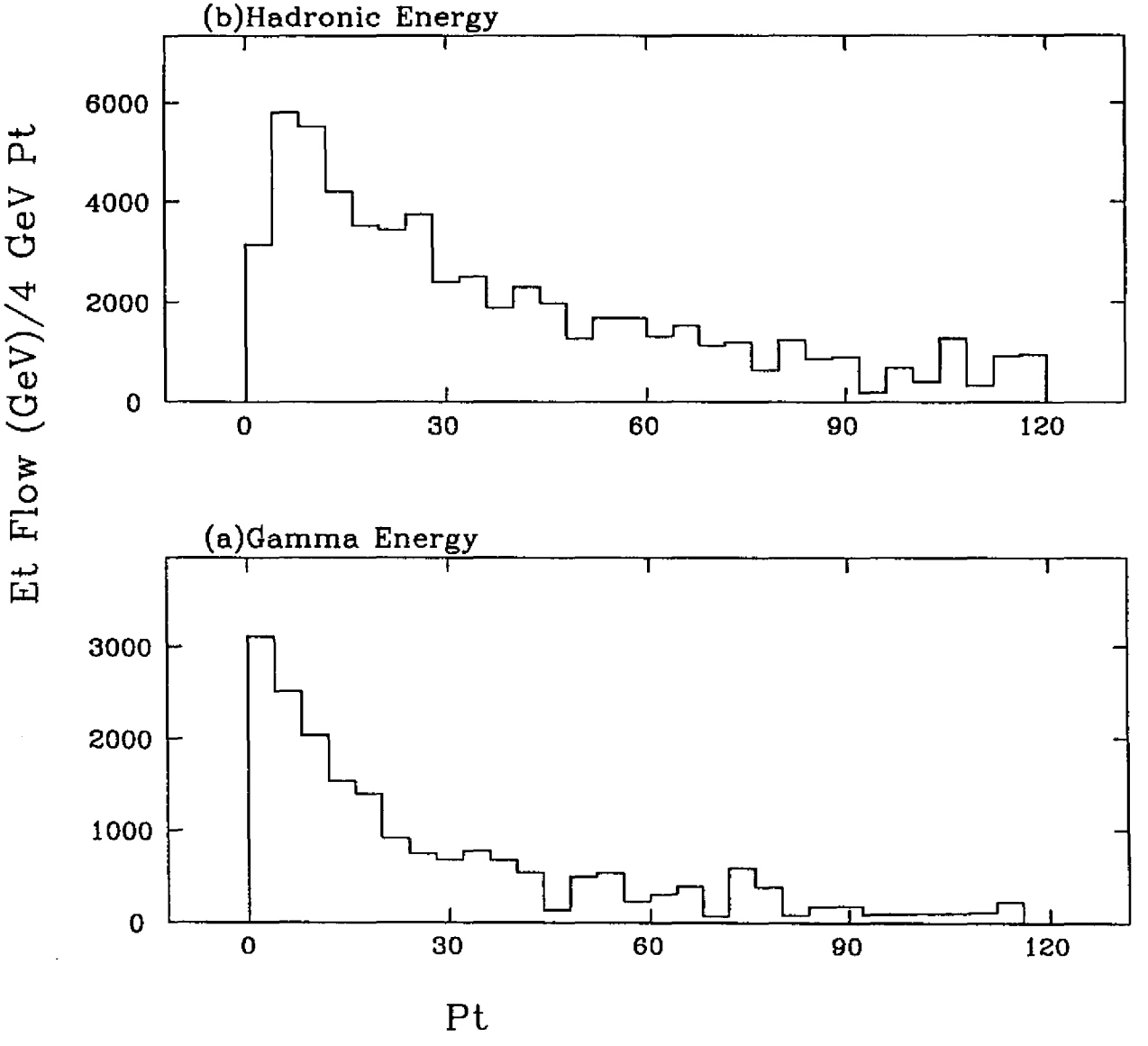
(b)Hadronic Energy
6000
4000
2000
0
0
30
60
90
120
Et Flow (GeV)/4 GeV Pt
(a)Gamma Energy
3000
2000
1000
0
0
30
60
90
120
Pt

Figure (2)

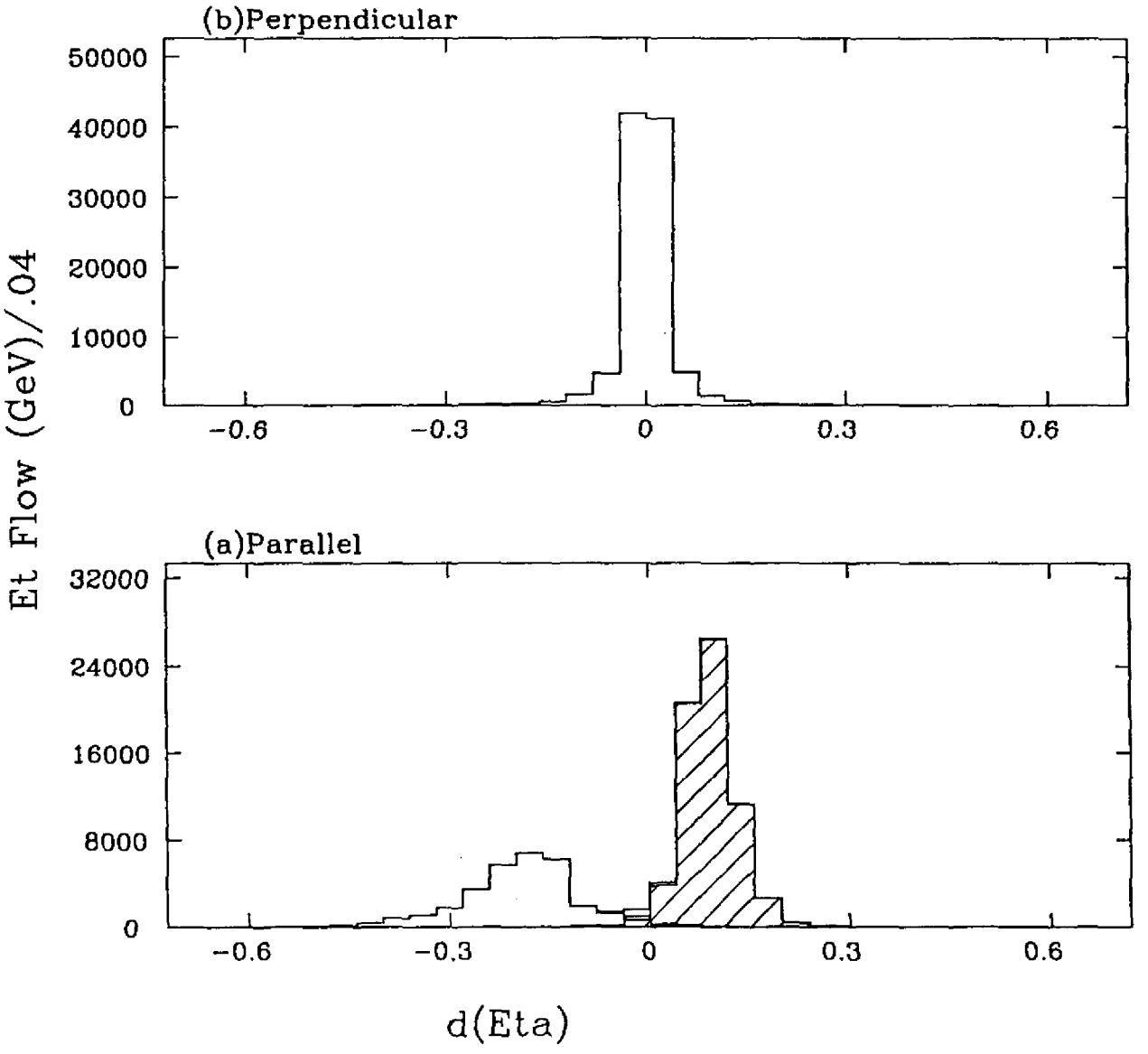
(b)Perpendicular
50000
40000
30000
20000
10000
0
-0.6
-0.3
0
0.3
0.6
Et Flow (GeV)/.04
(a)Parallel
32000
24000
16000
8000
0
-0.6
-0.3
0
0.3
0.6
d(Eta)

Figure (3)

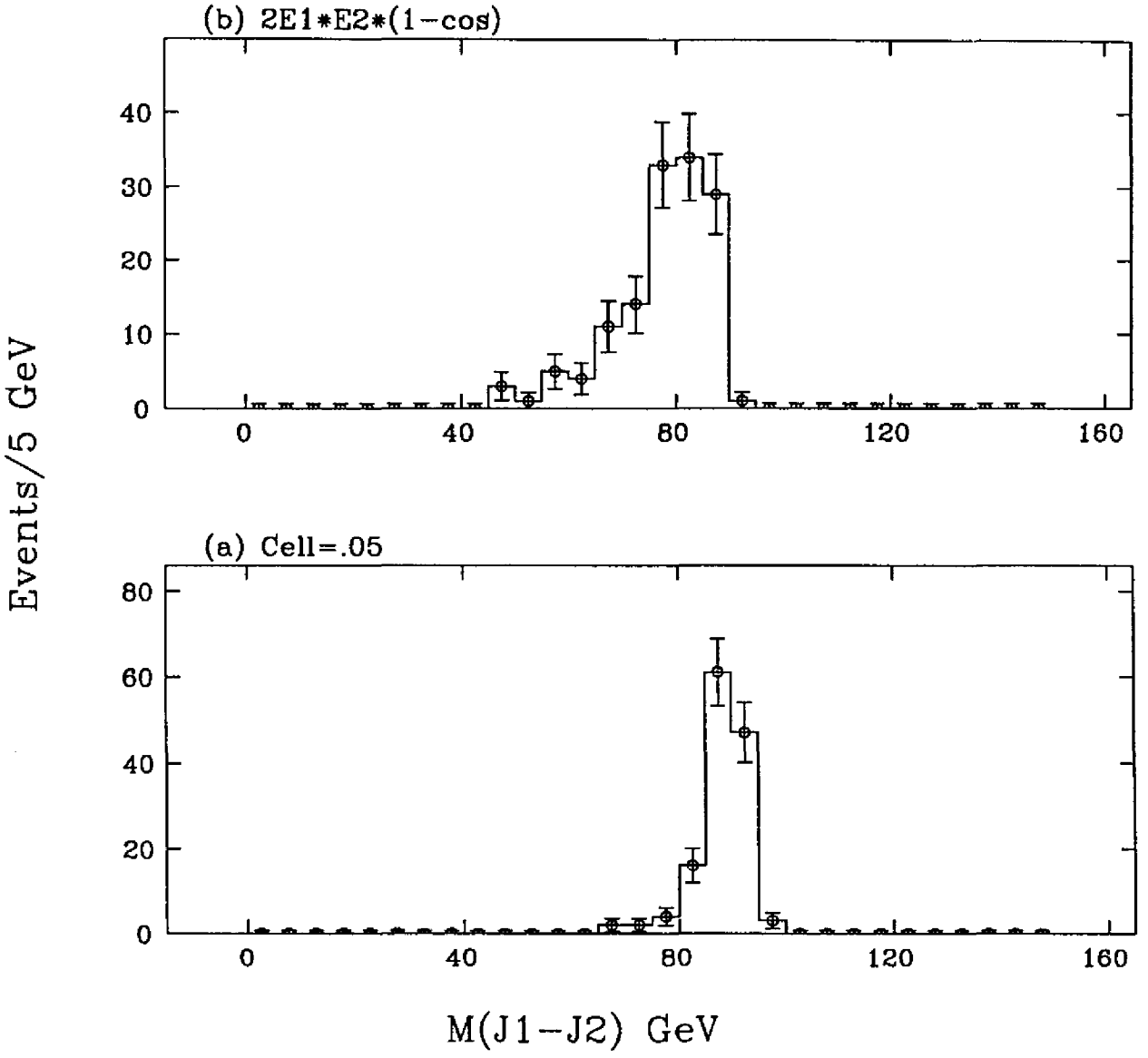
(b) 2E1*E2*(1-cos)
(a) Cell=.05
Events/5 GeV
M(J1-J2) GeV
0
10
20
30
40
0
20
40
60
80
0
40
80
120
160

Figure (4)

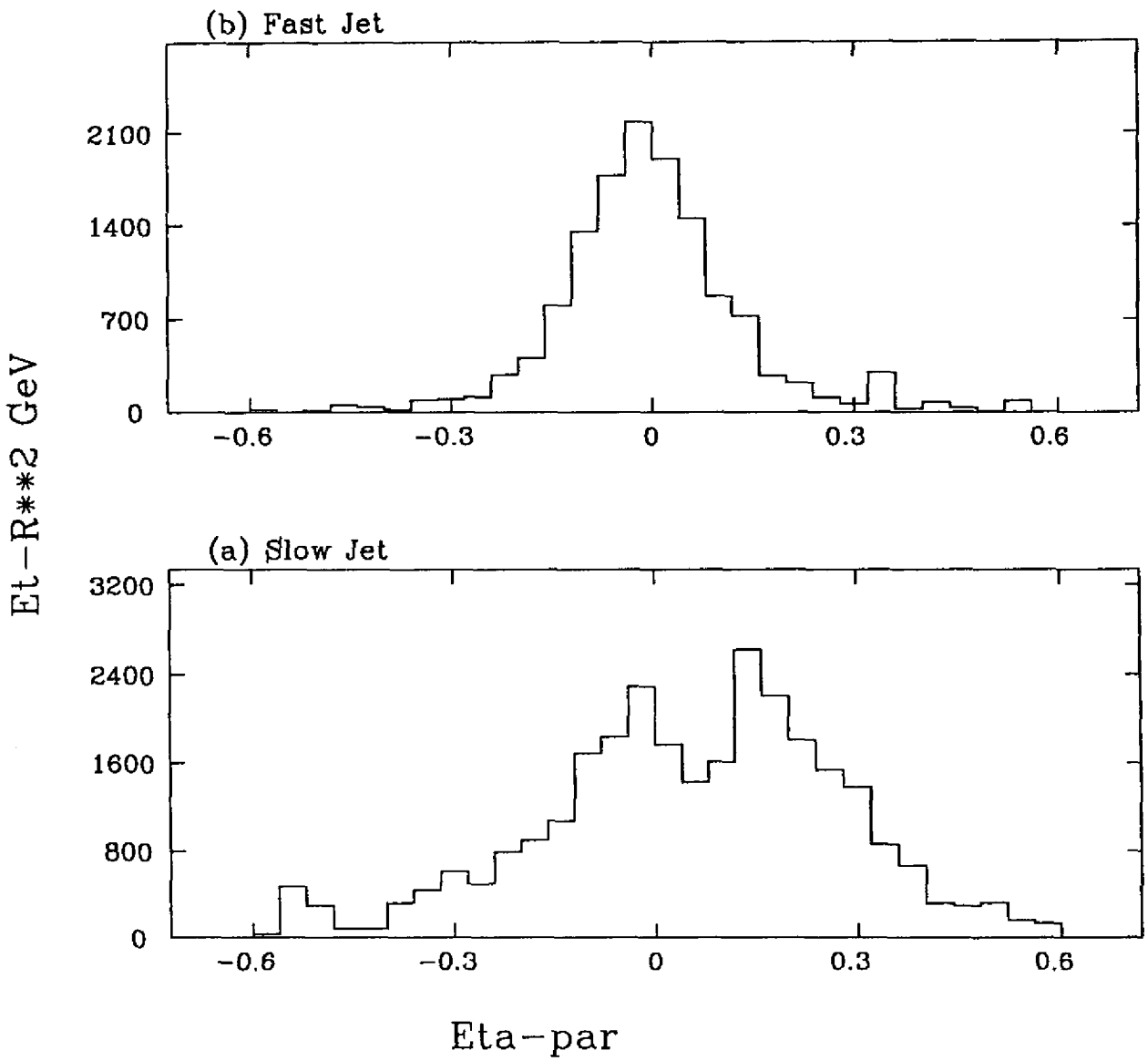
(b) Fast Jet
2100
1400
700
0
-0.6
-0.3
0
0.3
0.6
(a) Slow Jet
3200
2400
1600
800
0
-0.6
-0.3
0
0.3
0.6
Et-R**2 GeV
Eta-par

Figure (5)

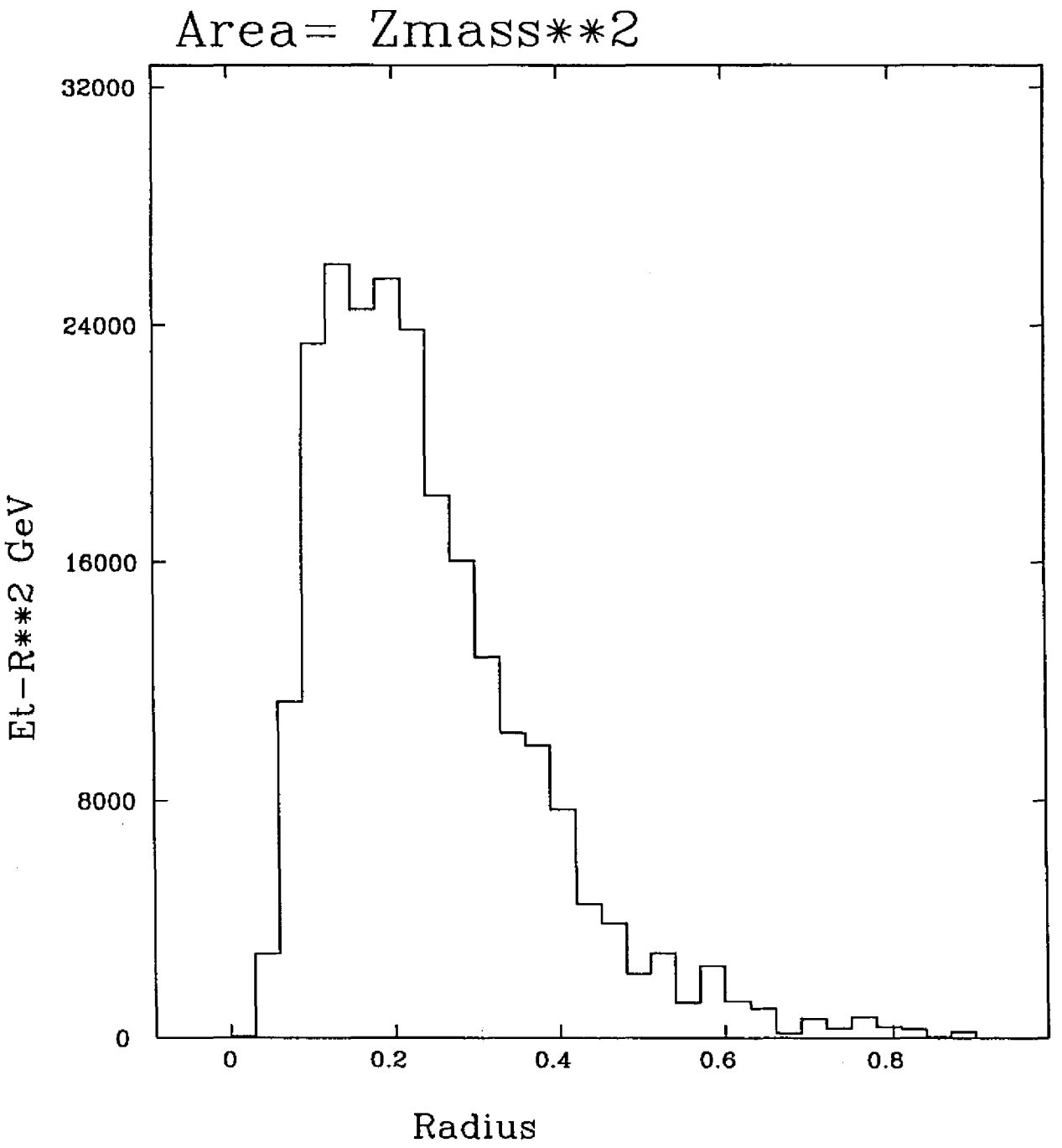
Area= Zmass**2
32000
24000
16000
8000
0
Et-R**2 GeV
0
0.2
0.4
0.6
0.8
Radius

Figure (6)

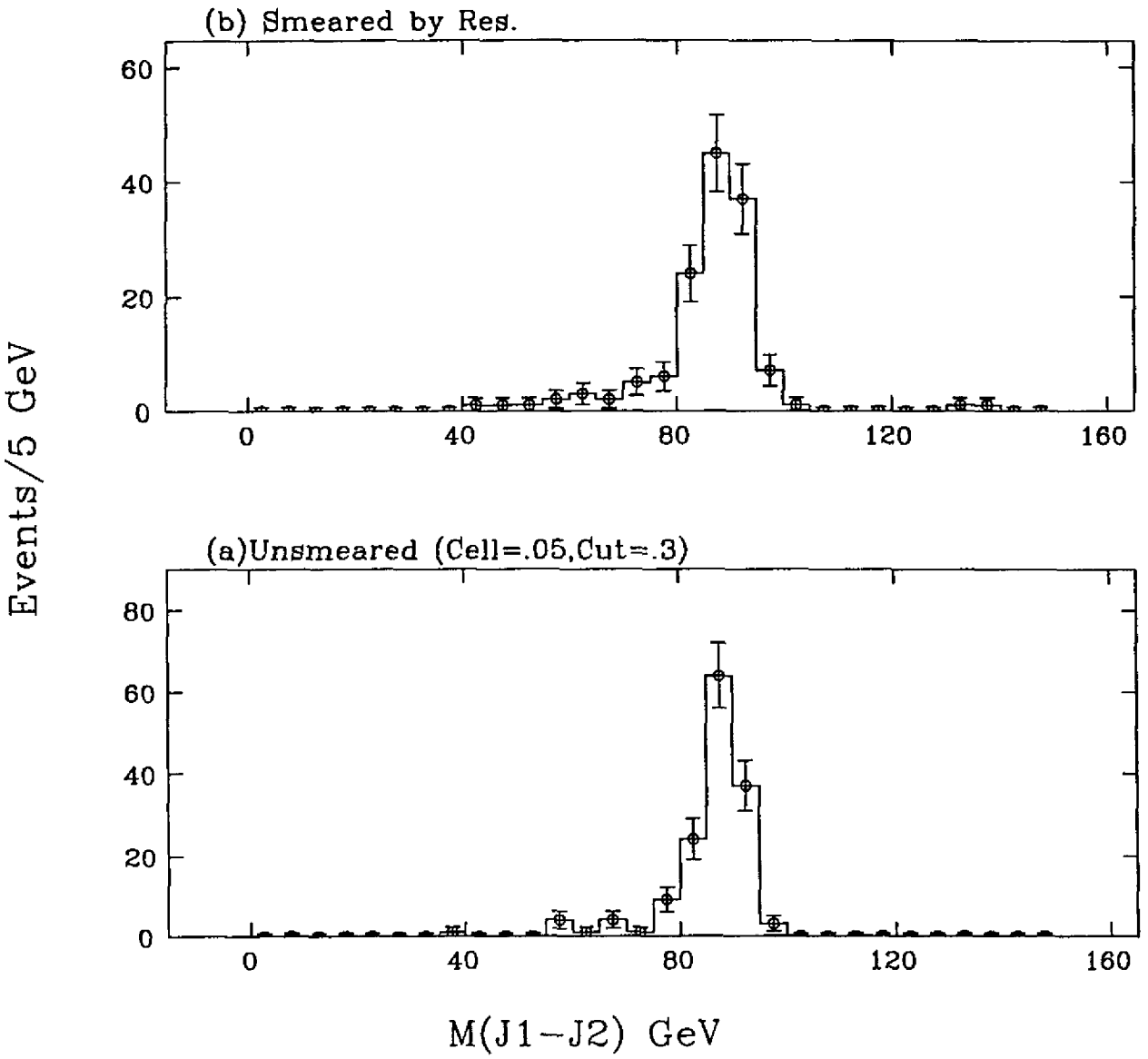
(b) Smeared by Res.
60
40
20
0
0
40
80
120
160
Events/5 GeV
(a)Unsmeared (Cell=.05,Cut=.3)
80
60
40
20
0
0
40
80
120
160
M(J1−J2) GeV

Figure (7)